

Abstract

WITH the aim to detect millimetric horizontal and vertical site displacements of geophysical origin, we investigate the problem of the propagation of electromagnetic GNSS signals through the troposphere. Our approach is to ray-trace the propagation, integrating the eikonal differential system through the atmospheric refractivity structures provided by the ECMWF model levels at all elevations and azimuths, and to characterize the delays by several mapping functions relative to each kind of physical processes perturbing the propagation. We especially focus on the lateral azimuthal variability of the propagation, and map the various processes describing the delays and ray bending by adapting suitable mapping functions at each time step. The Azimuthal Anisotropy Adaptive Mapping Functions, developed at GRGS Toulouse, summarize hundred thousands of rays in a few tens of coefficients at a few millimeters accuracy whatever the azimuth and for a five degrees elevation cutoff, and are suitable to correct GNSS signals at the measurement level.

1. Refractivity

THE refractivity of the moist air is the key parameter which drive the propagation of GNSS signals through the troposphere. The total refractivity of moist air may be expressed in terms of the (total moist air) pressure and the wet (water vapor) partial pressure.

$$N_k = k_1 \frac{P_k}{T_k} + \left(k_2' \frac{P_{vap,k}}{T_k} + k_3 \frac{P_{vap,k}}{T_k^2} \right) \quad (1)$$

This decomposition is preferred because its first term strictly follows the hydrostatic equilibrium of the model and the total refractivity does not depart too much from an hydrostatic equilibrium. The refractivity coefficients are empirically determined coefficients which depend on the frequency of the electromagnetic signals. The empirical refractivity coefficients are $k_1 = 77.6 \cdot 10^{-2} K \cdot Pa^{-1}$, $k_2 = 70.4 \cdot 10^{-2} K \cdot Pa^{-1}$ and the coefficient $k_2' = 22.1 \cdot 10^{-2} K \cdot Pa^{-1}$ is a combination of k_1 and k_2 , $k_3 = 3.739 \cdot 10^3 K^2 \cdot Pa^{-1}$ (Bevis et al. 1994).

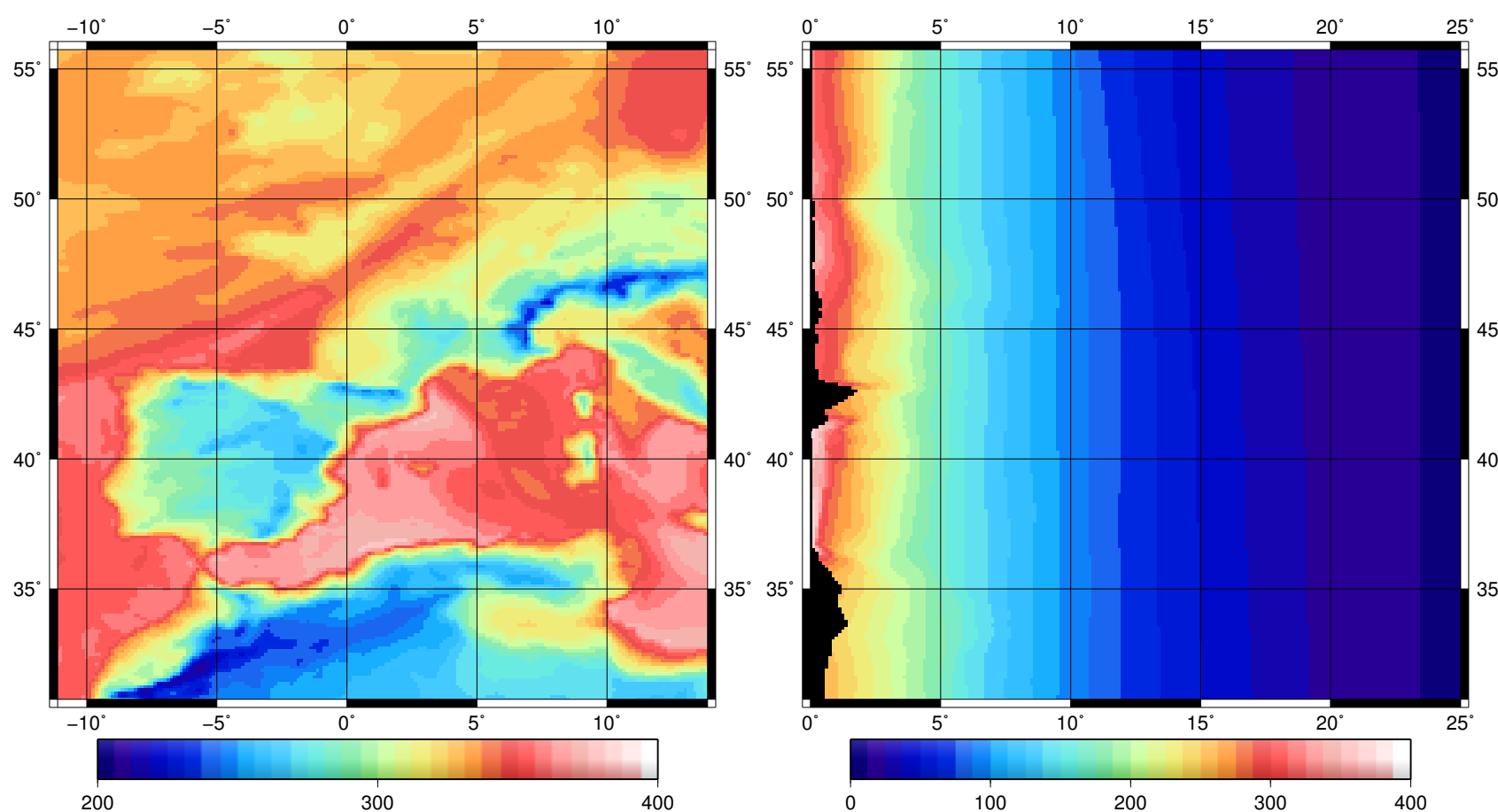


Figure 1: Surface refractivity N_{91} and Latitudinal vertical refractivity profile computed every 125m using the vertical refractivity functionals for the GPS tracking station located in Toulouse (08/10/2008, 16Z). The Latitude of the Toulouse site is $\phi = 43.36^\circ$ and the Longitude is $\lambda = 1.48^\circ$

Vertical refractivity functionals are introduced in order to properly represent the refractivity between the model levels along the normal to the ellipsoid which points to the zenith of the local horizon. Since the hydrostatic term strictly follows the hydrostatic equilibrium and since the vertical (total) refractivity profile is close to an hydrostatic profile, exponential functionals are chosen.

$$N(\phi_i, \lambda_j, z) = \exp(N_k^c + N_k^z) \quad \forall z \in [z_k, z_{k-1}] \quad (2)$$

$$N_k^c(\phi_i, \lambda_j) = (z_{k-1} \ln N_k - z_k \ln N_{k-1}) / (z_{k-1} - z_k) \quad (3)$$

$$N_k^z(\phi_i, \lambda_j) = (\ln N_{k-1} - \ln N_k) / (z_{k-1} - z_k) \quad (4)$$

Horizontal interpolations to the propagation path are required. For a point $P(\phi, \lambda, z)$ along the propagation path, the coefficients $N_k^c(\phi_i, \lambda_j)$ and $N_k^z(\phi_i, \lambda_j)$ of the four neighbouring refractivity profiles are interpolated by a bilinear interpolation to define the vertical refractivity profile by $N_p^c(\phi, \lambda)$ and $N_p^z(\phi, \lambda)$ at point P.

$$N(\phi, \lambda, z) = \exp(N_p^c(\phi, \lambda) + N_p^z(\phi, \lambda)z) \quad (5)$$

The refractive index $n(z)$ along the propagation path is

$$n(\phi, \lambda, z) = 10^{-6} N(\phi, \lambda, z) + 1 \quad (6)$$

The refractivity functional $N(\phi, \lambda, z)$ provide a continuous formulation of the vertical gradient of the refractive index.

$$\frac{dn}{dz} = (n-1)N_p^z \quad \text{with } z \in [z_k, z_{k-1}] \quad (7)$$

2. Propagation: The eikonal equation

DURING its propagation through the refractive atmosphere, GNSS electromagnetic waves are slowed down and their direction of propagation change depending on their own frequencies and the medium they propagate through. The physical propagation property is given by the empirical refractive index n which vary temporally and spatially with changing atmospheric conditions.

- The physical law governing the propagation is the eikonal equation. Paths followed by GNSS waves are geometrical rays which are perpendicular to the wavefronts. The eikonal equation lead to a set of non-linear partial differential equations, the characteristic equations, and is solved for the radio path length by the so-called method of characteristics. The characteristics are the geometrical rays.

- The arclength s and the travel time T are dependent variables which adjust so that the travel time along the geometrical ray is stationary accordingly to Fermat's principle. The spherical coordinates, the radial distance r , the geocentric colatitude θ and the longitude λ are relative to the frame linked to the Earth's center of mass.

The eikonal equation simply is $H(r, \theta, \lambda, p_r, p_\theta, p_\lambda) = 0$.

$$H = \frac{1}{2} \left(p_r^2 + \frac{p_\theta^2}{r^2} + \frac{p_\lambda^2}{r^2 \sin^2 \theta} - n^2(r, \theta, \lambda) \right) = 0 \quad (8)$$

The six first-order eikonal differential equations are deduced, by taking the longitude λ as the independent variable, to a set of five first-order eikonal differential equations describing the partials of the position of the current point $P(r, \theta, \lambda)$ along the ray path

$$\frac{dr}{d\lambda} = \frac{r \sin \theta \tan \varepsilon}{\sin \alpha} \quad \frac{d\theta}{d\lambda} = \sin \theta \cot \alpha \quad \frac{d\lambda}{d\lambda} = 1 \quad (9)$$

The partial derivatives of the elevation ε and the azimuth α :

$$\frac{d\varepsilon}{d\lambda} = \frac{\sin \theta}{\sin \alpha} \left(\frac{1}{n} \frac{dn}{dr} + 1 \right) + \frac{\sin \theta \tan \varepsilon}{\tan \alpha} \frac{1}{n} \frac{dn}{d\theta} + \tan \varepsilon \frac{1}{n} \frac{dn}{d\lambda} \quad (10)$$

$$\frac{d\alpha}{d\lambda} = -\cos \theta + \frac{\sin \theta}{\cos^2 \varepsilon n} \frac{dn}{d\theta} - \frac{\cot \alpha}{\cos^2 \varepsilon n} \frac{dn}{d\lambda} \quad (11)$$

Partial derivatives of the arclength of the ray s and the optical path length L of the wave through the dense atmosphere are added to the eikonal differential system to provide the required solution.

$$\frac{ds}{d\lambda} = \frac{r \sin \theta}{\cos \varepsilon \sin \alpha} \quad \frac{dL}{d\lambda} = n \frac{r \sin \theta}{\cos \varepsilon \sin \alpha} \quad (12)$$

An additional partial derivative relative to the hydrostatic delay D_h is required to estimate separately the hydrostatic and the non-hydrostatic terms.

$$\frac{dD_h}{d\lambda} = \bar{n} \frac{r \sin \theta}{\cos \varepsilon \sin \alpha} \quad (13)$$

3. Delays

THE arclength L_S is simply the geometrical length of the ray. The radio path length L account for an increase of length due to the wave propagating at a speed $v = c/n$, in the medium of refractive index $n > 1$, slower than the speed of light c it would have in vacuum, and for an increase of the arclength L_S of the ray path S , relative to the bending of the ray path due to the gradients of the refractive index, in comparison to the straight line path S_L it would follow in vacuum. The radio path length is the solution of the propagation problem but is developed in terms of the hydrostatic and non-hydrostatic terms. The sum of this two terms is the total delay.

$$L = \int_S ds + \int_S (n_h - 1) ds + \int_S (n_{nh} - 1) ds \quad (14)$$

The geometric delay D_G is defined as the difference in length of the paths S and S_L , the arclength L_S minus the geometric distance of the straight line L_G .

$$D_G = L_S - L_G = \int_S ds - \int_{S_L} ds \quad (15)$$

The radio delay D is defined as the increase of length of the optical length L compared to the straight line distance or geometric distance L_G between the starting and ending points of the ray path.

$$D = L - L_G = \int_S n ds - \int_{S_L} ds \quad (16)$$

4. Anisotropy Adaptive Mapping Functions

ADAPTIVE Mapping Functions are now defined. The basic underlying idea is to insert a dependency to the azimuth α inside each fraction coefficient a_{i_f} that is introducing a Fourier serie in α :

$$a_{i_f} = a_{i_f,0} + \sum_{i_\alpha=1}^{i_\alpha=n_\alpha} a_{i_f,i_\alpha}^c \cos i_\alpha \alpha + a_{i_f,i_\alpha}^s \sin i_\alpha \alpha \quad (17)$$

The numerator and denominator at fraction truncation are

$$N_{n_f} = 1 + a_{n_f} \quad D_{n_f} = \sin \varepsilon + a_{n_f} \quad (18)$$

The numerator and denominator at each level index i_f are

$$N_{i_f} = 1 + a_{i_f}/N_{i_f+1} \quad D_{i_f} = \sin \varepsilon + a_{i_f}/D_{i_f+1} \quad (19)$$

These recursive definitions lead to the numerator N_f and denominator D_f of the mapping function f .

$$N_f = 1 + \frac{a_1}{1 + \frac{a_2}{1 + \dots}} \quad D_f = \sin \varepsilon + \frac{a_1}{\sin \varepsilon + \frac{a_2}{\sin \varepsilon + \dots}} \quad (20)$$

And the mapping function f is scaled by a scaling factor S_f . The elevation mapping function f^ε is a specific case.

$$f = S_f \frac{N_f}{D_f} \quad f^\varepsilon = f \cos \varepsilon \quad (21)$$

As the usual mapping function $f_{3,0}(\varepsilon)$ truncated at the third fraction $n_f = 3$ does not depend on α ($n_\alpha = 0$),

$$f = S_f \frac{1 + \frac{a_1}{1 + \frac{a_2}{1 + a_3}}}{\sin \varepsilon + \frac{a_1}{\sin \varepsilon + \frac{a_2}{\sin \varepsilon + a_3}}} \quad (22)$$

the adaptive mapping function $f_{3,1}(\varepsilon, \alpha)$ truncated at the third fraction $n_f = 3$ with α -series truncated at the first term $n_\alpha = 1$ is

$$N_{f_{3,1}} = 1 + \frac{a_{1,0} + a_{1,1}^c \cos \alpha + a_{1,1}^s \sin \alpha}{1 + \frac{a_{2,0} + a_{2,1}^c \cos \alpha + a_{2,1}^s \sin \alpha}{1 + \frac{a_{3,0} + a_{3,1}^c \cos \alpha + a_{3,1}^s \sin \alpha}} \quad (23)$$

$$D_{f_{3,1}} = \sin \varepsilon + \frac{a_{1,0} + a_{1,1}^c \cos \alpha + a_{1,1}^s \sin \alpha}{\sin \varepsilon + \frac{a_{2,0} + a_{2,1}^c \cos \alpha + a_{2,1}^s \sin \alpha}{\sin \varepsilon + \frac{a_{3,0} + a_{3,1}^c \cos \alpha + a_{3,1}^s \sin \alpha}} \quad (24)$$

Gradients are introduced in two alternative forms: a formulation where the gradient is embedded in the fraction form by addition of four terms in the fraction coefficient a_1 or the classical formulation.

$$a_1^g = a_1 + (E_c^c \cos \alpha + E_c^s \sin \alpha) \cos \varepsilon \quad (25)$$

$$+ (E_t^c \cos \alpha + E_t^s \sin \alpha) \tan \varepsilon \quad (26)$$

$$\text{or } f = S_f \frac{N_f}{D_f} (1 + (D^c \cos \alpha + D^s \sin \alpha) \cot \varepsilon) \quad (27)$$

5. Classical Mapping Functions

CLASSICAL mapping functions F3A0C5G2 are defined without dependency in azimuth except for the classical gradient. Even with a modified scale of the residuals graph which is 2 cm instead of 2 mm, residuals below ten degrees residuals are greater. The same conclusion is reached if the fraction contains 5 terms (F5A0C5G2). The classical gradient is not able to capture the azimuthal anisotropy.

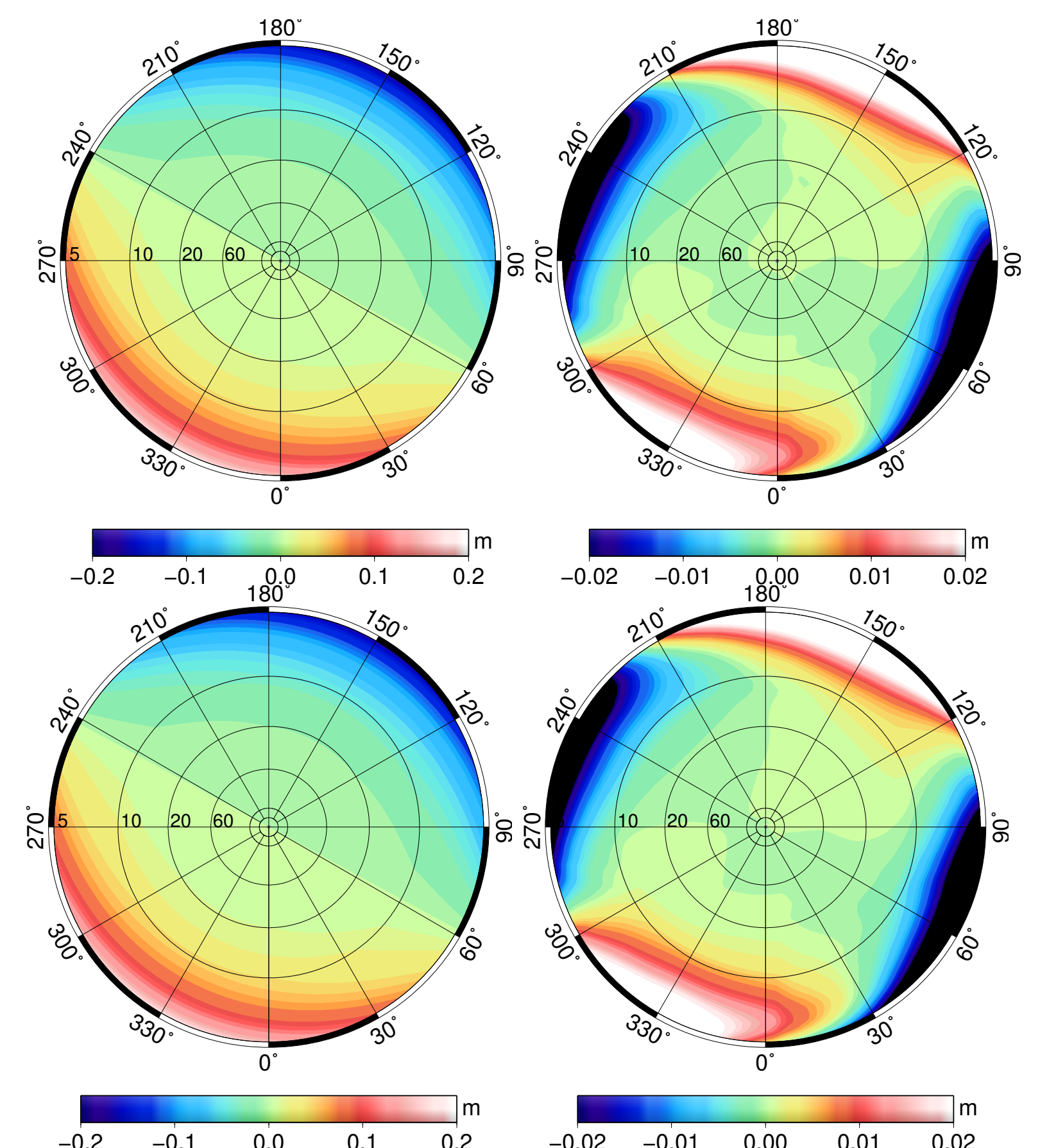


Figure 2: Anisotropy (left) and residuals (right) of the delay mapped by the Classical Mapping Function F3A0C5G2 $n_f = 3$ (up) or F5A0C5G2 $n_f = 5$ (down) without azimuthal terms $n_\alpha = 0$ and with the classical gradient formulation.

6. Performance of Adaptive Mapping Functions

HOW do specific adaptive mapping functions perform to fit rays to mapping functions with a suitable accuracy? Several fraction truncations and α -series truncations are now tested.

A convention is useful to name specific mapping functions:

- F3 is the fraction truncation number $n_f = 3$,
- A4 is the truncation of the series at $n_\alpha = 4$,
- C5 is the elevation cutoff at 5 degrees,
- G2 is the two terms classical gradient and
- G4 is the embedded gradient formulation.

Introducing the first two terms of the Fourier series $n_\alpha = 2$ F3A2C5G2 (Figure 3), residuals drop below the millimeter level above 10° , but below, some regions exhibit residuals above 5 mm. Although the truncation to $n_f = 5$ slightly improve the fit, large residuals are present (F5A2C5G2).

Introducing a higher fraction truncation allow the elevation profile of the functional to have more inflexion points and to be bended with different slopes especially at low elevation where the fourth and fifth fractions are significant.

The following graph shows that order of truncation higher than 2 of the Fourier serie in α are required.

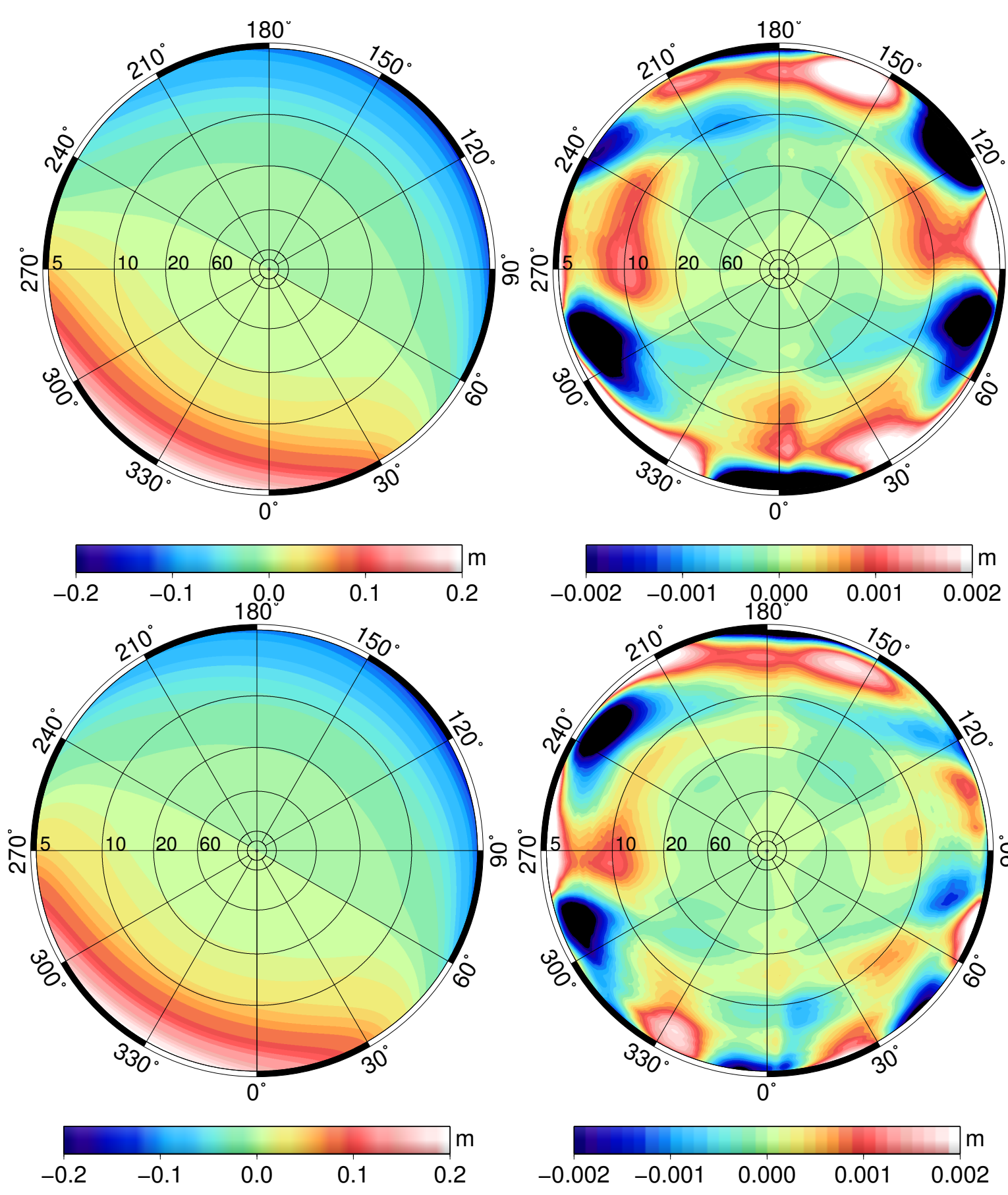


Figure 3: Anisotropy (left) and residuals (right) of the tropospheric delay mapped by the Adaptive Mapping Function F3A2C5G2 $n_f = 3$ (up) or F5A2C5G2 $n_f = 5$ (down) with the α -serie truncated at $n_\alpha = 2$ and with the classical gradient formulation.

The α -serie truncated at order $n_\alpha = 4$ now contains 8 azimuthal terms per fraction. The AMF-F3A4C5G2 contains 27 coefficients, 2 terms for the gradient and 1 for the scale factor (Figure 4). The scale factor is close to the zenith delay but may differ in some special cases (not shown) if the minimum of the delays is not at the zenith.

When the α -series are truncated at order 4, Residuals are now less than two millimeters for F3A4C5G2 and less than one millimeter for F5A4C5G2.

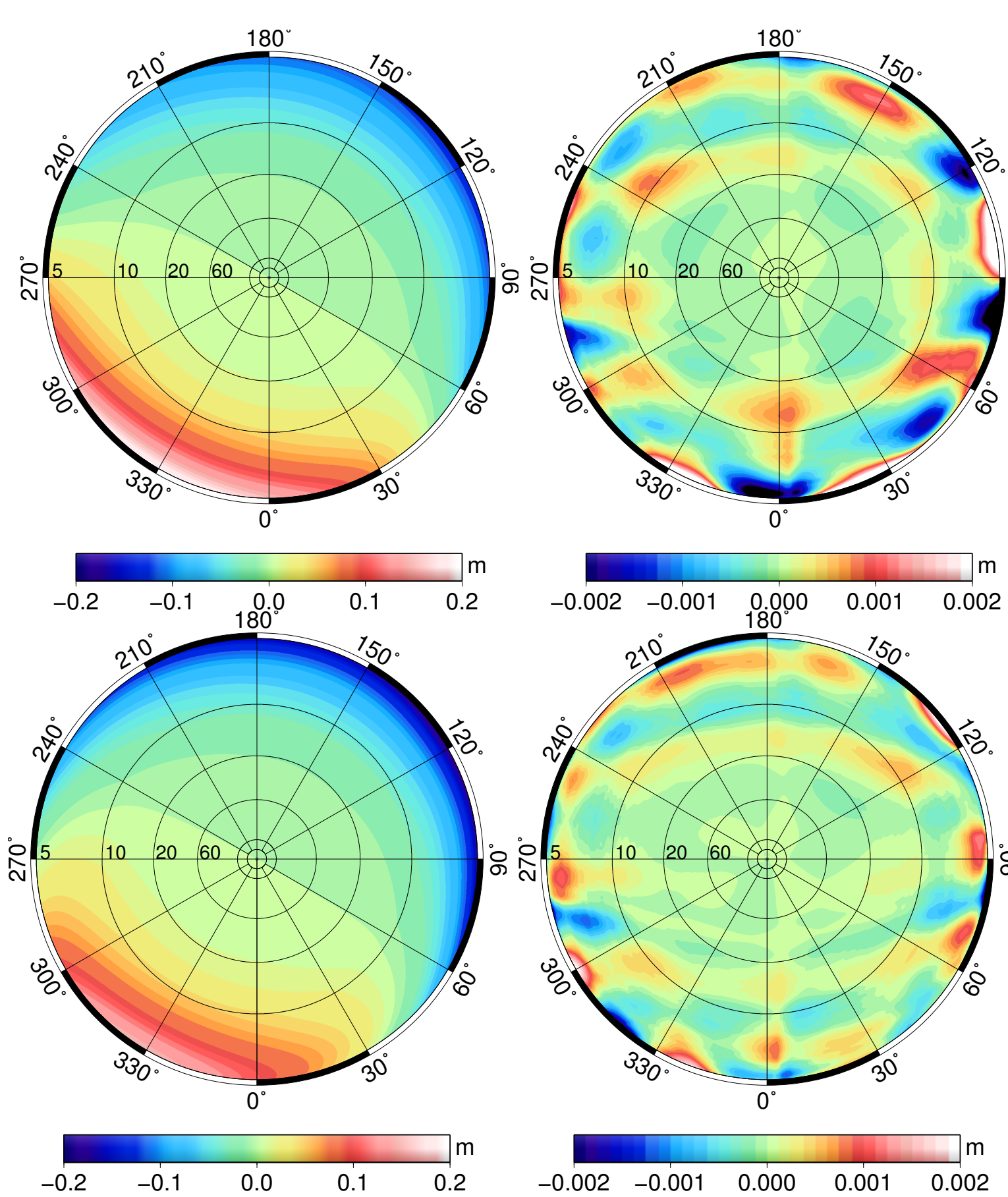


Figure 4: Anisotropy (left) and residuals (right) of the tropospheric delay mapped by the Adaptive Mapping Function F3A4C5G2 $n_f = 3$ (up) or F5A4C5G2 $n_f = 5$ (down) with the α -serie truncated at $n_\alpha = 4$ and with the classical gradient formulation.

The embedded gradient slightly improve the fit but not significantly enough (Figure 5). We conclude that the use of the adaptive mapping function containing 3 fractions and a fourier serie in α truncated at $n_\alpha = 4$ allow to fit 32,400 rays above an elevation cutoff of 5° using 30 coefficients with an acceptable accuracy.

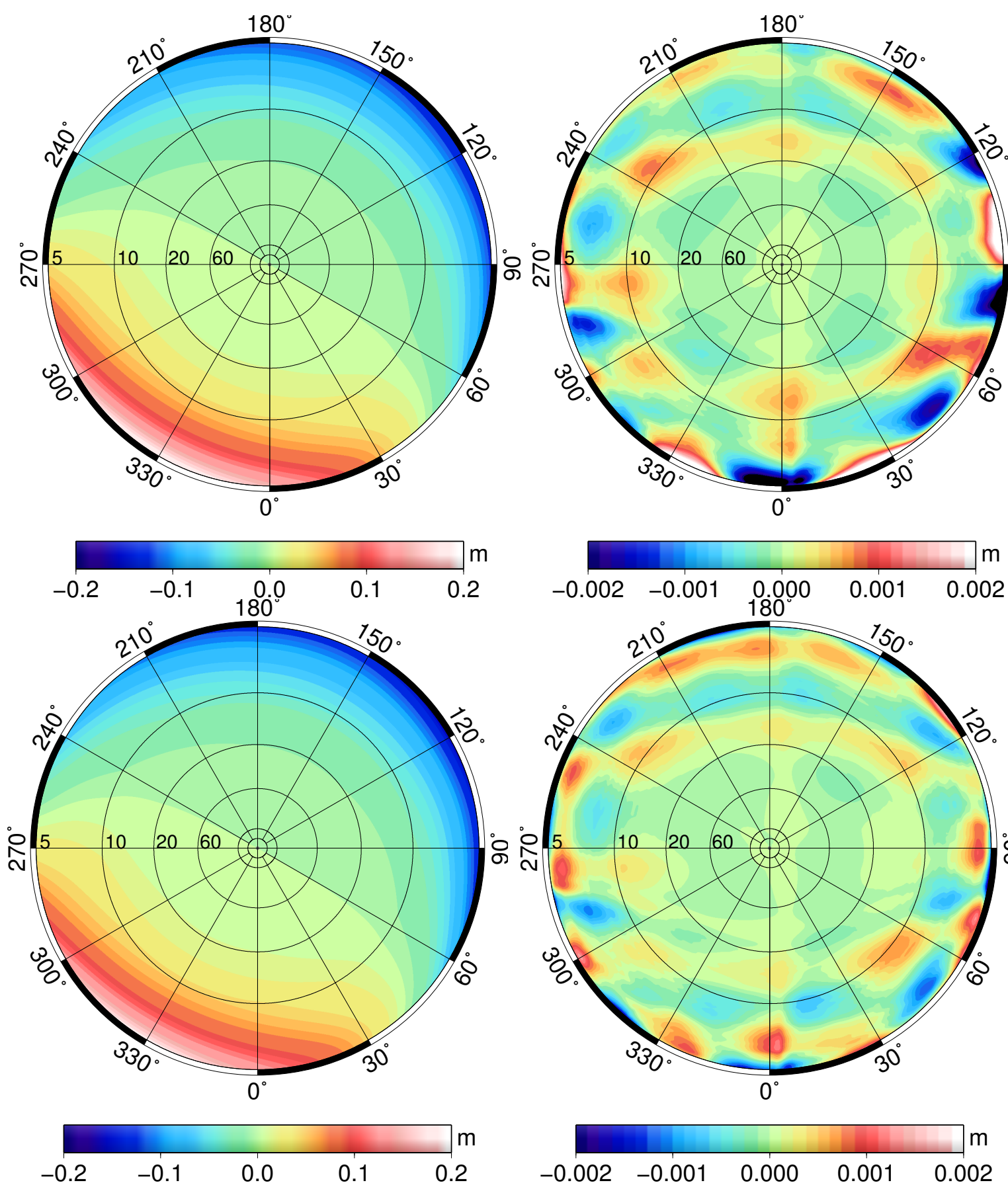


Figure 5: Anisotropy (left) and residuals (right) of the tropospheric delay mapped by F3A4C5G4 $n_f = 3$ (up) or F5A4C5G4 $n_f = 5$ (down) with the α -serie truncated at $n_\alpha = 4$ and the embedded gradient formulation.

7. Mapping Elevations and Delays

THE following figures provide mapping examples of the components of the tropospheric delay and the elevation function using the AMF-F3A4C5G2. The elevation bending variability represented on Figure 6 has an amplitude of 0.004 degree which seems small compared to a bending of 0.2 degree at a 5° elevation. But an error on the elevation angle of 0.004 degree which is the main parameter of the delay mapping function would lead to an error of 16 mm! It is therefore crucial to account for the azimuthal variability by introducing an elevation bending mapping function to accurately estimate the incident elevation angle at the site.

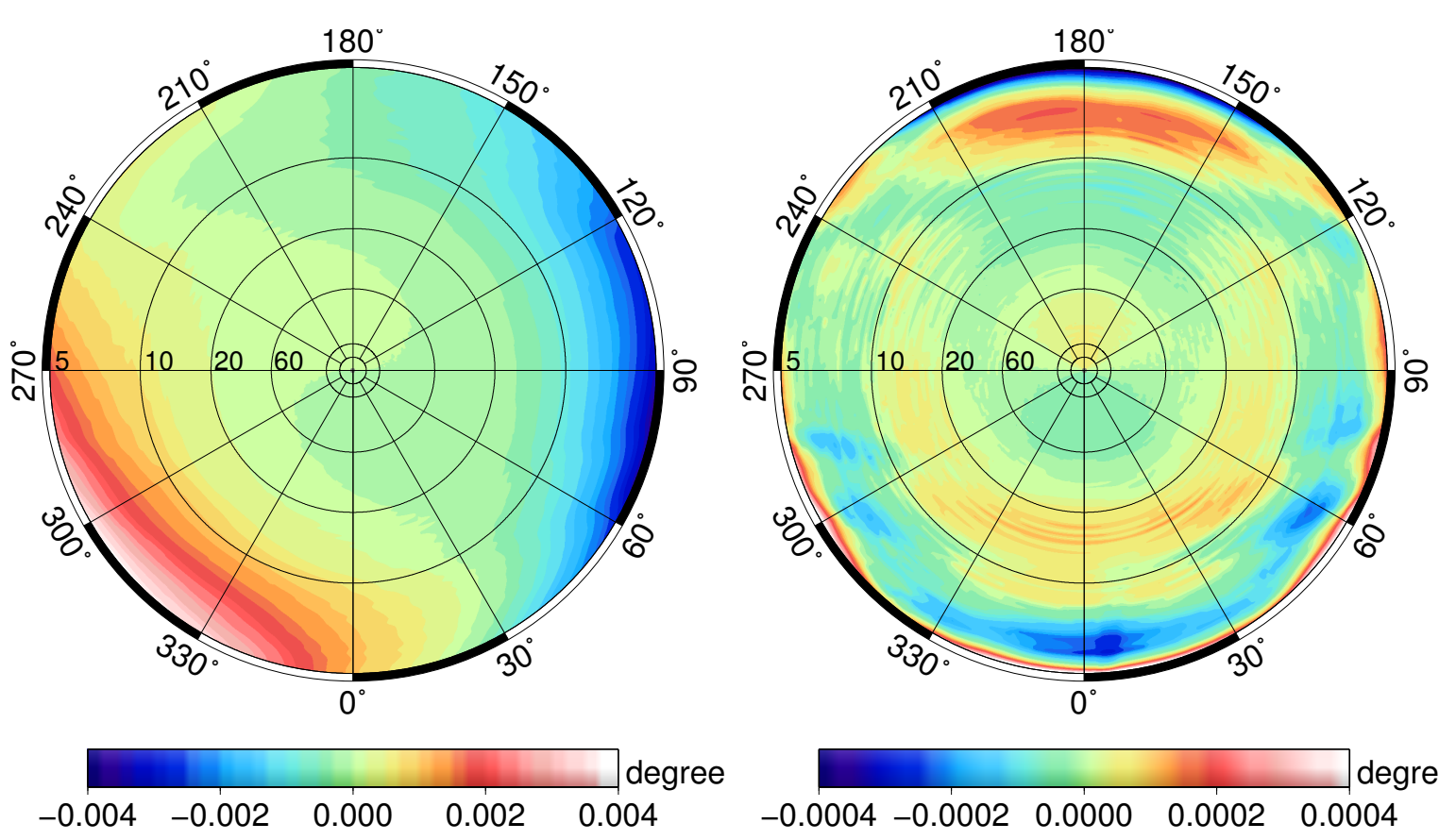


Figure 6: Fit of the anisotropy (left) and residuals (right) of the elevation bending $\Delta\varepsilon$ by a F3A4C5G2 Adaptive Mapping Function at Toulouse in August 10, 2008, 16Z

The AMF-R-F3A4C5G2 and AMF-T-F3A4C5G2 fit respectively the tropospheric radio delay and the total delay (non-hydrostatic + hydrostatic delays) (see Figure 7). The difference between these two delays is the geometric delay which is here calculated at the top of atmosphere but has to be computed in fine at the satellite position using the solution to the parallax problem. The geometric delay is ten times smaller than the total delay. Small differences can be seen at azimuths 60° or 150° at 6° elevation.

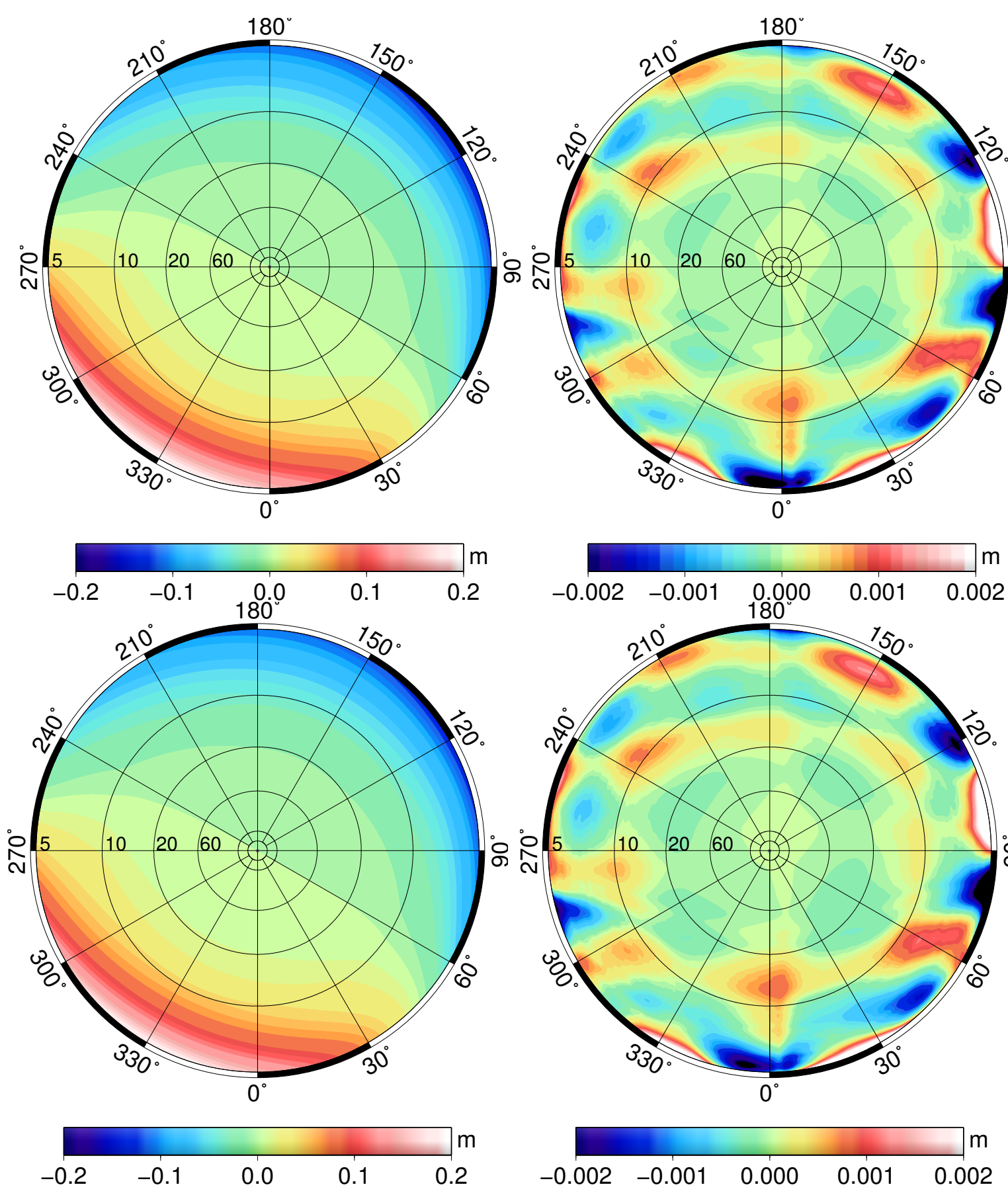


Figure 7: Fitted azimuthal variability (left) and residuals (right) of the radio delay AMF-R-F3A4C5G2 (up) and the total delay AMF-T-F3A4C5G2 (down) by a F3A4C5G2 adaptive mapping function at Toulouse in 08/10, 16Z

The AMF-N-F3A4C5G2 fit the non-hydrostatic delay (Fig. 8). Localized residuals does not exceed 2 mm. The AMF-H-F3A4C5G2 fit the hydrostatic delay with a similar accuracy. The azimuthal anisotropy of the non-hydrostatic term is the main contributor to the total azimuthal anisotropy. For this case study, the azimuthal anisotropy pattern is explained by the dry air over Spain at azimuth 330° from the Toulouse site when at the same time air containing more moisture can be observe over France (Figure 1) in the opposite direction.

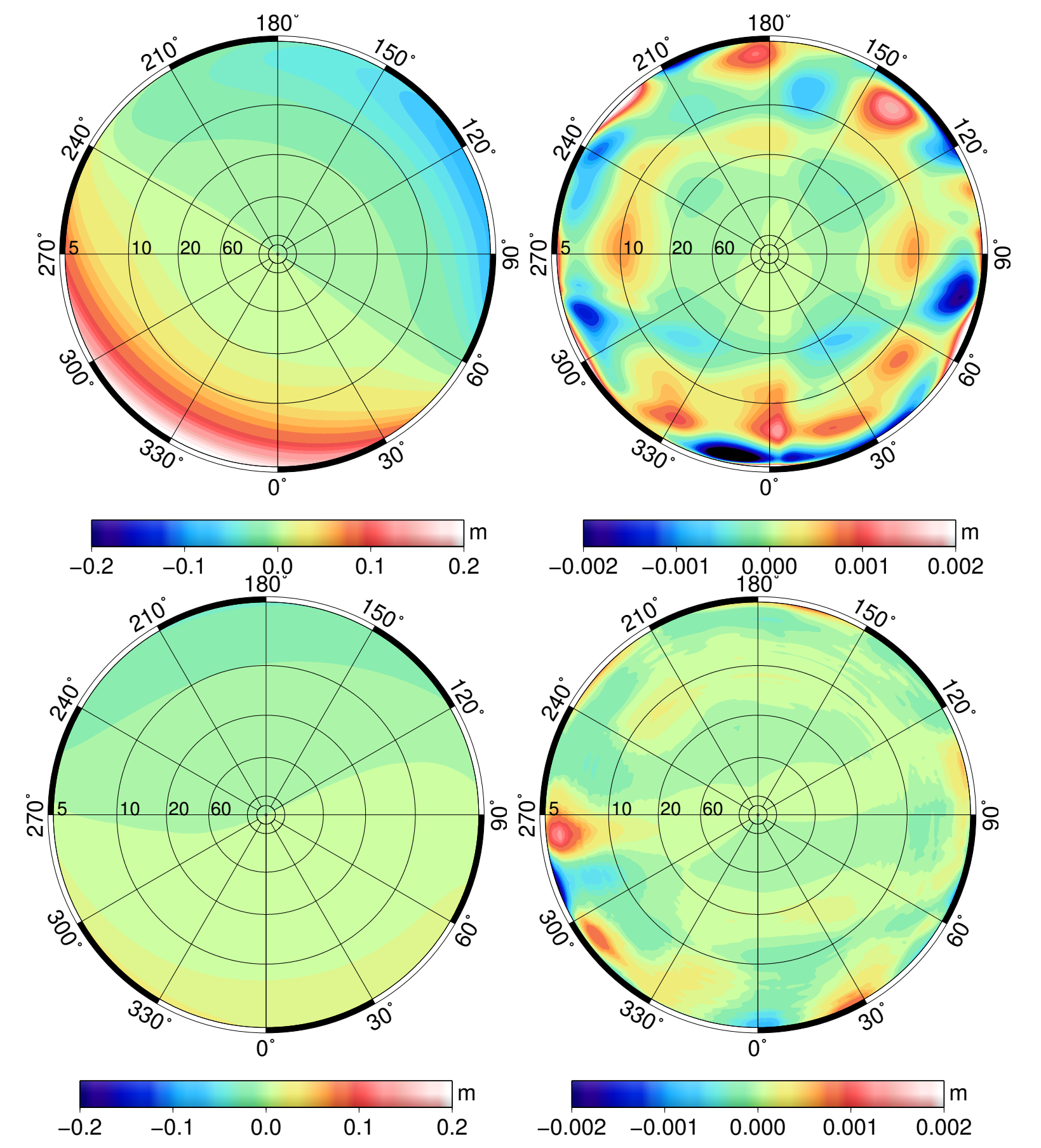


Figure 8: Fitted azimuthal variability (left) and residuals (right) of the non-hydrostatic AMF-N-F3A4C5G2 (up) and hydrostatic AMF-H-F3A4C5G2 (down) delays calculated for the Toulouse GPS station, August 10, 2008, 16Z

In the perpendicular direction (60°), a symmetric distribution of moist air over the Atlantic ocean and the Mediterranean Sea does not generate (a dissymetry) a large gradient (this is not the case 4 hours later, Figure 9).

8. Time discretisation

Several interpolation scheme may be investigated but the key point is the time variability of delays itself. Similarly to what is observed in the time-variable gravity field modeling, the propagation patterns are mainly driven by the solar radiation patterns (thermal tides) and to a smaller extent by the regional (600 km around the site) meteorological systems. Figure 9 present the time variability of the anisotropic part of the tropospheric delay using an hourly dataset. The hourly samples of this day show smooth variations in anisotropy except between 9Z+5 and 9Z+7 where the patterns are completely inverted in two hours. A 6-hourly sampling is done by looking only at the first column of the skyplots. It would lead to a misrepresentation (usual aliasing) of semi-diurnal processes! A 3-hourly sampling seems better but would lead to a bad representation of what is happening between 09Z+03 and 09Z+09! **These figures reveal the usefulness of increasing the time discretisation of meteorological processes for space geodetic applications.**

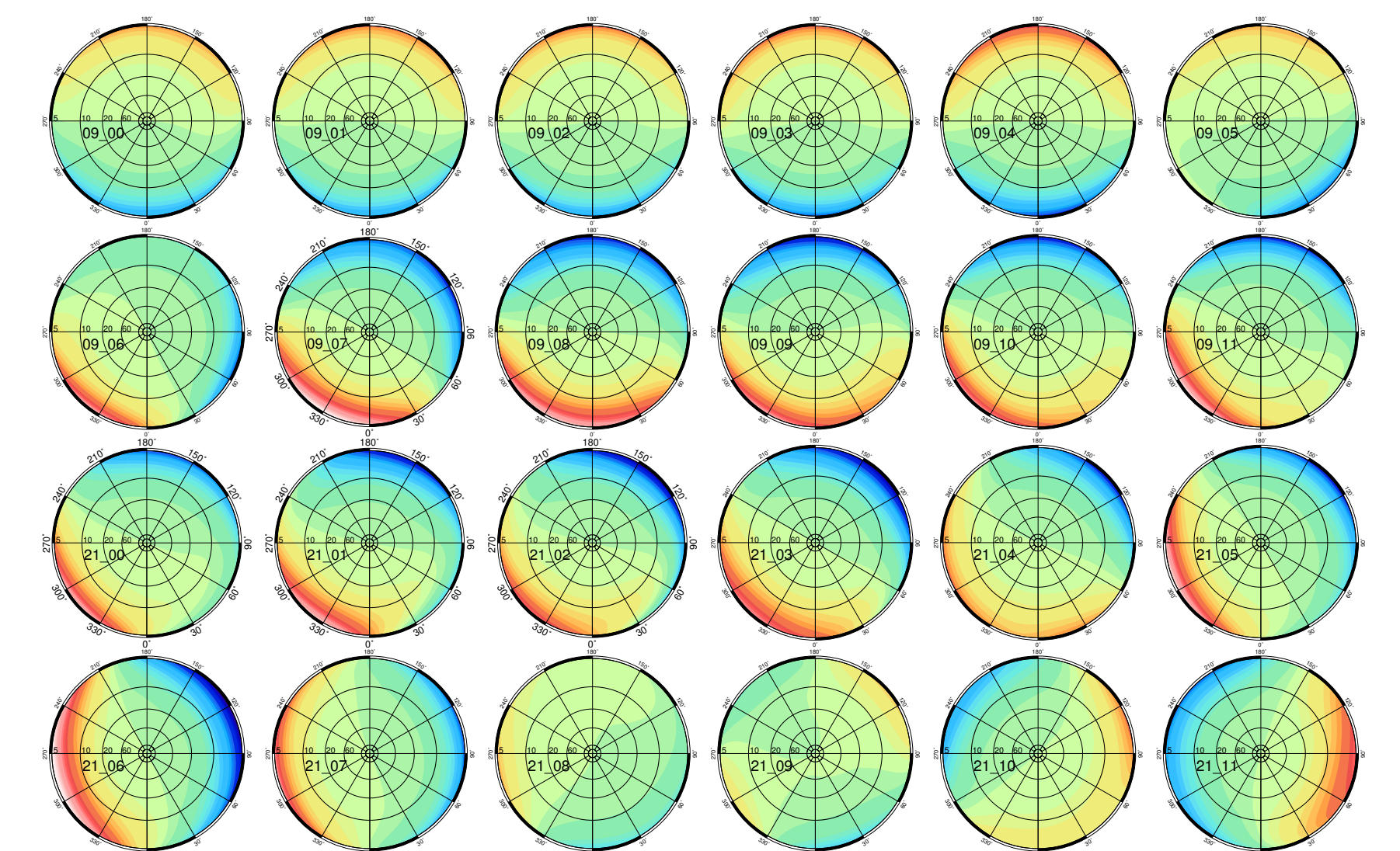


Figure 9: Fitted azimuthal anisotropy of the tropospheric radio delay in Toulouse for 24 hourly steps beginning at 09Z, August 10, 2008.

Practical investigations of a large number of situations and sites are required to provide a realistic accuracy of the estimated delays depending on interpolation and sampling. Time discretization of the delays relies on the meteorological archives but it remains a major issue for the modeling of tropospheric delays from numerical weather models.

9. Conclusions

SINCE the tropospheric delays are very sensitive to elevation, especially at low elevation, we underline that the parallax problem has to be properly solved (not shown). At 5° elevation, an inappropriate deviation of 0.25° would lead to a metric error! Determining the proper ray elevation at the site is as critical as properly fitting the azimuthal anisotropy because all corrections depend on this angle. **This study provide a detailed discussion of some physical and mathematical formulations needed to maintain as far as possible a millimetric accuracy in handling the atmospheric model, tracing rays, fitting mapping functions and solving the parallax problem.** Although the millimetric accuracy is a concern which motivates the introduction of some formulations, the time discretization may not guarantee such precision and further investigations are required. Undergoing statistical investigation of a large number of meteorological situations depending on the site and practical orbitographic studies should provide realistic estimates of the performance of the presented method.